Spiral phase and spin waves in the quasi-two-dimensional antiferromagnet $Ba_2CuGe_2O_7$

A. Zheludev and G. Shirane
Brookhaven National Laboratory, Upton, New York 11973-5000

Y. Sasago, N. Kiode, and K. Uchinokura
Department of Applied Physics, The University of Tokyo, 7-3-1 Hongo, Bunkyo-ku, Tokyo 113, Japan
(Received 1 March 1996; revised manuscript received 12 June 1996)

The quasi-two-dimensional square-lattice antiferromagnet $Ba_2CuGe_2O_7$ was studied by neutron scattering and bulk magnetic techniques. An incommensurate magnetic spiral structure with the propagation vector $(1+\zeta,1+\zeta,0)$ ($\zeta=0.027$) was observed below $T_N=3.26$ K. Magnetic ordering occurs with a two-dimensional-like critical exponent $\beta\approx0.15$. The spin dynamics can be adequately described by conventional spin-wave theory with two exchange constants: nearest-neighbor in-plane antiferromagnetic coupling $J_1\approx0.48$ meV and interplane ferromagnetic interaction $J_\perp\approx0.013$ meV. This set of exchange parameters apparently fails to explain the spiral order. The noncentrosymmetric crystal structure suggests that the incommensurate phase may be the result of a Dzyaloshinskii-Moriya instability of the Néel ground state.
[S0163-1829(96)07546-7]

I. INTRODUCTION

The discovery of a spin-singlet ground state in $CuGeO_3$ (Refs. 1 and 2) inspired experimentalists to look for model low-dimensional magnetic systems among transition metal germanates and silicates. The strategy turned out to be very successful and recently led to the discovery of spin-singlet ground state in $CaCuGe_2O_6$.[3,4] In our quest for investigating new low-dimensional systems we have performed the synthesis, bulk magnetic measurements and neutron scattering studies of $Ba_2CuGe_2O_7$. The magnetism of this compound is due to $S=1/2$ spins localized on the Cu^{2+} sites that are all crystallographically equivalent. The tetragonal crystal structure[5] [space group $P\bar{4}2_1m$ (No. 113), lattice constants $a=8.466$ Å, $c=5.445$ Å] is noncentrosymmetric, but otherwise shows a high degree of symmetry. Unlike the pronounced chain structure of $CaCuGe_2O_6$, the characteristic feature of $Ba_2CuGe_2O_7$ is a square-lattice arrangement of Cu^{2+} ions in the (a,b) crystallographic plane [Fig. 1(a)] with the possibility of superexchange interactions via the GeO_4 tetrahedra along the diagonals [first nearest neighbor (1NN)] and possibly the sides (2NN) of the (a,b)-projected unit cell (Fig. 2). Adjacent Cu-planes are separated by layers of Ba with no obvious superexchange routes [Fig. 1(b)]. These structural features suggest that the material may exhibit quasi-two-dimensional behavior and, possibly, competing 1NN and 2NN in-plane antiferromagnetic interactions. It is the simple square-lattice spin arrangement that makes $Ba_2CuGe_2O_7$ particularly interesting. In addition, the value $S=1/2$ guarantees that the magnetic properties will not be influenced by single-ion anisotropy and also allows us to expect strong quantum effects.

In this paper we report magnetic susceptibility measurements and inelastic neutron scattering experiments on $Ba_2CuGe_2O_7$. At first only powder samples were available for our studies. Diffraction experiments failed to detect any long-range magnetic ordering down to $T=1.4$ K. At this temperature inelastic measurements revealed a distinct broad peak in the magnetic excitation spectrum at $\hbar\omega\approx1.6$ meV. The position of the inelastic feature was found to be Q independent within the experimentally accessible range of momentum transfer. At that time the observed behavior was interpreted as evidence of a spin-singlet ground state and spin gap in $Ba_2CuGe_2O_7$.[6] Recently large high-quality

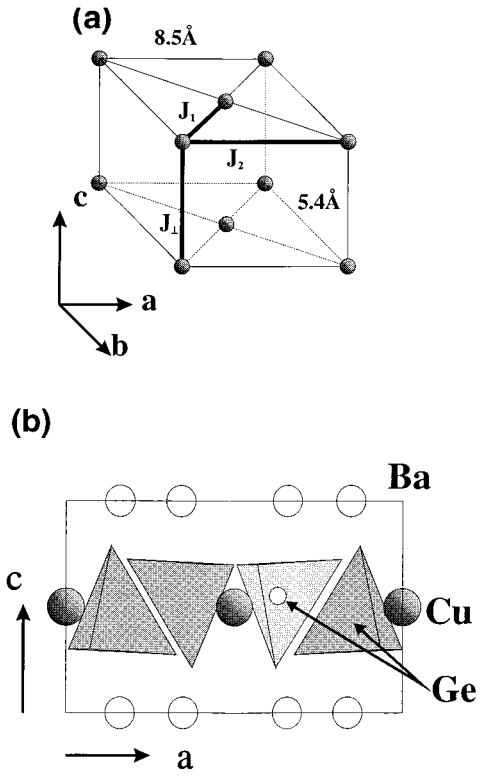

FIG. 1. (a)Arrangement of Cu^{2+} ions in $Ba_2CuGe_2O_7$. Solid lines indicate the potential in-plane (J_1 and J_2) and out-of-plane ($J_\perp$) exchange constants. (b) Crystal structure of $Ba_2CuGe_2O_7$ in projection onto the (a,c) plane, showing the GeO_4 tetrahedra.

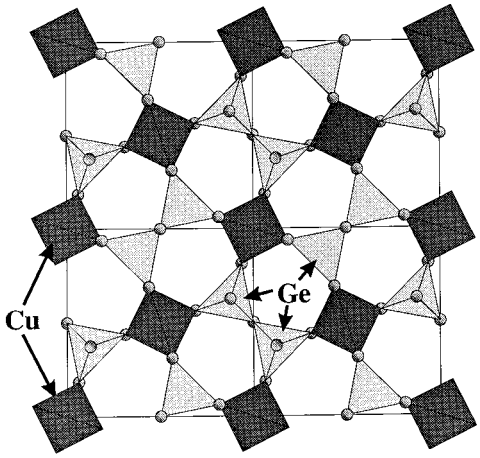

FIG. 2. Crystal structure of $Ba_2CuGe_2O_7$ in projection onto (a,b) plane. Ba ions are not shown. Cu and Ge sites are represented by coordination tetrahedra.

single crystals of the compound became available. Single crystal neutron scattering experiments described in this paper revealed a picture very different from that previously concluded from powder measurements. We show that below $T_N=3.3$ K $Ba_2CuGe_2O_7$ undergoes a transition to a bulk magnetically ordered state and no gap is present in the magnetic excitation spectrum. The low-temperature magnetic phase is a magnetic *spiral* with the propagation vectors $(1\pm\zeta,1\pm\zeta,0)$, $\zeta\approx0.027$. The strongly two-dimensional (2D) spin wave dispersion is measured and quantitatively analyzed. The relevant exchange constants are obtained. The experimental results are discussed in connection to several theoretical constructs.

II. EXPERIMENTAL

$Ba_2CuGe_2O_7$ powder samples were fabricated by ordinary solid-state reaction method. The temperature dependence of the bulk magnetic susceptibility $\chi(T)$ was measured using a standard ac SQUID magnetometer in the temperature range 2–300 K and in a constant applied field of 1000 Oe on a 56.8 mg powder sample. A $15\times10\times6$ mm^3 translucent pale-yellow single crystal sample for neutron work was grown using the floating-zone method. The sample was of excellent quality with an isotropic mosaic spread of $\approx20'$, as measured by neutron diffraction.

Neutron scattering experiments were carried out on the H4m, H7, H8 (thermal beam) and H9 (cold source) three-axis spectrometers at the High Flux Beam Reactor (HFBR) at Brookhaven National Laboratory on the single crystal described above and a 8.0 g powder samples. The use of a standard ''ILL orange'' cryostat and a two-stage Displex refrigerator allowed us to perform the measurements in the range 1.4–300 K. Several spectrometer configurations were exploited. In all cases pyrolitic graphite (PG) (0 0 2) reflections were used as monochromator and analyzer. Measurements with a fixed initial neutron energy $E_i=14.7$ meV were carried out on H4m, H7, and H8 using $(40'-40'-40'-40')$ or $(20'-40'-20'-40')$ collimations (setups A and B) and two PG filters in front of the

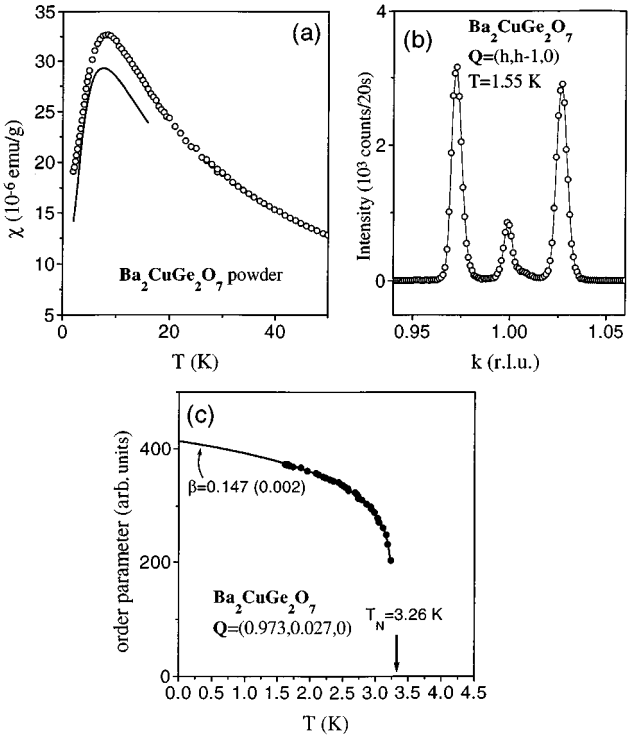

FIG. 3. (a) Temperature dependence of the magnetic susceptibility of a $Ba_2CuGe_2O_7$ powder. The solid line is a theoretical prediction for a 2D Heisenberg antiferromagnet with nearest-neighbor interactions (Refs. 7 and 8). (b) Elastic scan along $(h,h-1,0)$ measured in the single crystal $Ba_2CuGe_2O_7$ sample at $T=1.55$ K, showing two magnetic Bragg peaks at incommensurate positions. The central component is temperature independent and was shown to be produced by double scattering (nonmagnetic). (c) Temperature dependence of the magnetic order parameter in $Ba_2CuGe_2O_7$ (solid circles) as deduced from the behavior of the (0.973,0.973,0) magnetic peak. The solid line represents a power-law fit.

sample. On H9 $(60'-40'-60'-\text{sample}-80'-80')$ collimations and $E_i=4.6$ meV were used with a Be filter in front of the sample (setup C). Inelastic powder data were collected at H7 with a fixed initial neutron energy $E_i=13.0$ meV and either $(40'-40'-40'-80')$ (setup D) or $(20'-40'-20'-80')$ (setup E) collimations and a PG filter in front of the sample. Most of the data were obtained in constant-Q energy scans. In these measurements the software driving the three-axis spectrometers automatically adjust the monitor rating to compensate for the changing analyzer efficiency and ''(k'/k)'' corrections. As a result, the observed intensity is directly proportional to the dynamic structure factor $S(\mathbf{q},\omega)$ of the scatterer.

III. RESULTS

A. Magnetic properties

1. Bulk magnetic susceptibility

Figure 3(a) shows the temperature dependence of the magnetic susceptibility measured in the $Ba_2CuGe_2O_6$ powder sample. The experimental curve was found to be similar to that theoretically predicted for a 2D Heisenberg antiferro-

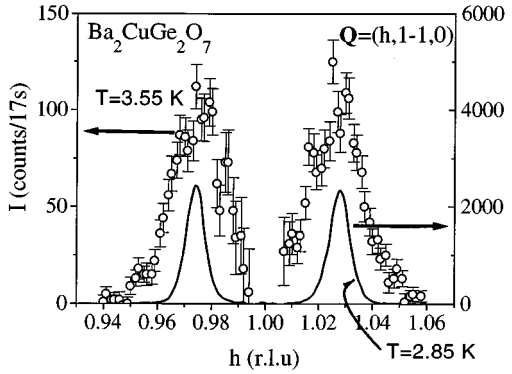

FIG. 4. Magnetic critical scattering observed in the $Ba_2CuGe_2O_7$ single-crystal sample using setup C at $T=3.55$ K $>T_N$ (open circles). The solid line shows magnetic Bragg peaks observed at $T=2.85$ K$<T_N$. In both curves the background measured at $T=5$ K has been subtracted.

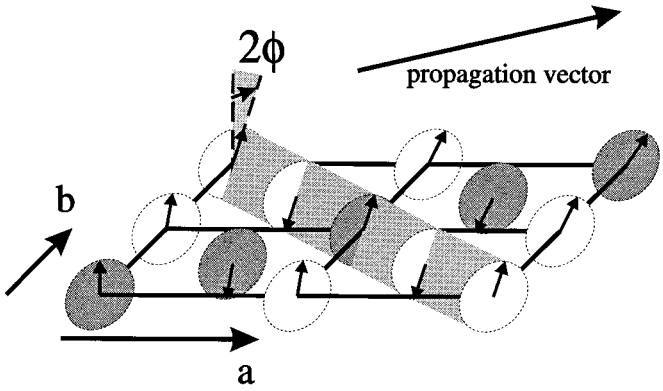

FIG. 5. Proposed model for the magnetic structure of $Ba_2CuGe_2O_7$. The spins lie in the $(1,-1,0)$ crystallographic plane. Upon translation along $(0.5,0.5,0)$ the spins rotate by an angle $\phi=9.7°$. Nearest-neighbor spins in adjacent $(0,0,1)$ planes are aligned parallel to each other.

magnet with nearest neighbor interactions.[7,8] In calculating the latter we have utilized gyromagnetic ratios deduced from single-crystal ESR measurements:[9] $g_{\|c}=2.07$ and $g_{\perp c}=2.45$, respectively.

2. Magnetic phase transition

Long-range magnetic ordering manifests itself in the apparition of magnetic Bragg reflections at incommensurate positions $(h\pm\zeta,k\pm\zeta,l)$ (h, k, l-integer, $h+k$-odd) below $T_N=3.26$ K [Fig. 3(b)]. The incommensurability parameter $\zeta=0.027$ was found to be constant in the entire studied temperature range. No higher-order reflections (such as $(h\pm2\zeta,k\pm2\zeta,l)$ were observed. $(h\pm\zeta,k\pm\zeta,l)$ (h, k, l-integer, $h+k$-even) reflections are also absent. The temperature dependence of the $(1-\zeta,1-\zeta,0)$ magnetic Bragg intensity was measured using setup C. The associated order parameter is plotted against T in Fig. 3(c). The data were analyzed by fitting it to a power law $(T_N-T)^{\beta}$. The best fit is obtained with $T_N=3.26$ K and the critical exponent $\beta=0.15(0.01)$ [solid line in Fig. 3(c)]. Critical scattering was plainly observed at $T>T_N$ around the $(h\pm\zeta,k\pm\zeta,l)$ (h, k, l-integer, $h+k$-odd) positions (Fig. 4). Accurate measurements of the critical exponent ν, that characterizes the temperature dependence of the magnetic correlation length, are yet to be performed.

3. Structure factor

The observed magnetic Bragg intensity pattern may be accurately reproduced by the following simple model (Fig. 5). All spins in the system lie in one plane. The relative spin alignment is ferromagnetic along $(0,0,1)$ and antiferromagnetic along $(1,-1,0)$ directions. A translation along $(0.5,0.5,0)$ induces a rotation of the spins (relative to an antiferromagnetic arrangement) by an angle ϕ in spin space ($\phi=0$ corresponds to nearest-neighbor Néel order). The incommensurability parameter ζ is given by $\zeta=\phi/2\pi$. In the tetragonal structure four types of magnetic domains with propagation vectors $(\pm\zeta,\pm\zeta,0)$ (as seen from the antiferromagnetic zone center at $(1,0,0)$) are possible. A simple structure-factor calculation shows that each domain with the propagation vector $(\zeta,\zeta,0)$ gives rise to two types of in-plane magnetic Bragg peaks, at $(h+\zeta,k+\zeta,0)$ and $(h-\zeta,k-\zeta,0)$ ($h+k$-odd), each with its own neutron polarization factor. Assuming that in a macroscopic sample ''ζ'' and ''$-\zeta$'' domains are equally represented, we obtain the following expression for the intensities of magnetic Bragg peaks:

$$\frac{d\sigma}{d\Omega}=\frac{1}{2}S^2g^2(\gamma r_0)^2N\frac{(2\pi)^3}{v_0}|f(q)|^2(1+\sin^2(\psi)). \quad (1)$$

Here N is the number of unit cells in the sample, v_0 is the unit cell volume, $(\gamma r_0)^2=0.291$ b, and $f(q)$ is the magnetic form factor for Cu^{2+}. ψ denotes the angle between the scattering vector and plane that contains the spins.

4. Magnetic structure

Bragg intensities of seven magnetic reflections measured using setup A at $T=1.6$ K in the $(h,k,0)$ plane, with h and k ranging from -3 to 3, were analyzed using formula (1), separately for each domain type. The intensity was normalized by the calculated volume of the resolution ellipsoid and put to the absolute scale (barn per unit cell) by comparing them to the measured intensities of several nuclear Bragg peaks. Experimentally, magnetic reflections of the types $(h-\zeta,k-\zeta,0)$ and $(h+\zeta,k+\zeta,0)$ have equal intensities and thus Eq. (1) is justified. The form factor for Cu^{2+} was taken from Ref. 10. Three models consistent with tetragonal symmetry, with the spins lying in the $(0,0,1)$, $(\zeta,\zeta,0)$, and $(\zeta,-\zeta,0)$ planes, respectively, were considered. Only one of these models, namely the one in which the spins lie and rotate in the $(1,-1,0)$ plane [for $(\zeta,\zeta,0)$ propagation vector] is consistent with the experimental data. At $T=1.6$ K the order parameter (by convention, unity if all the spins are strictly arranged in spirals) was found to be ≈0.8. This shows that all the spins in the system are properly accounted for by the proposed model.

B. Inelastic neutron scattering

The measurements of the spin wave dispersion relation for energy transfers $(\hbar\omega)\gtrsim0.8$ meV were performed using

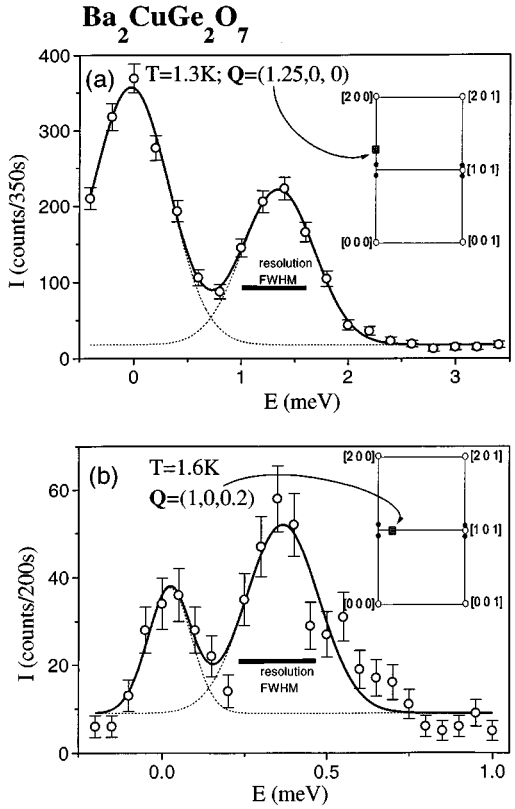

FIG. 6. Typical inelastic constant-Q scans for the single crystal $Ba_2CuGe_2O_7$ sample measured at $\mathbf{Q}=(1.25,0,0)$ using experimental setup A (a) and at $\mathbf{Q}=(1,0,0.2)$ using setup C (b). The inserts schematically show the positions in Q space where the scans were taken (open and solid circles mark the nuclear and magnetic Bragg reflections, respectively). In both panels lines represent empirical Gaussian fits.

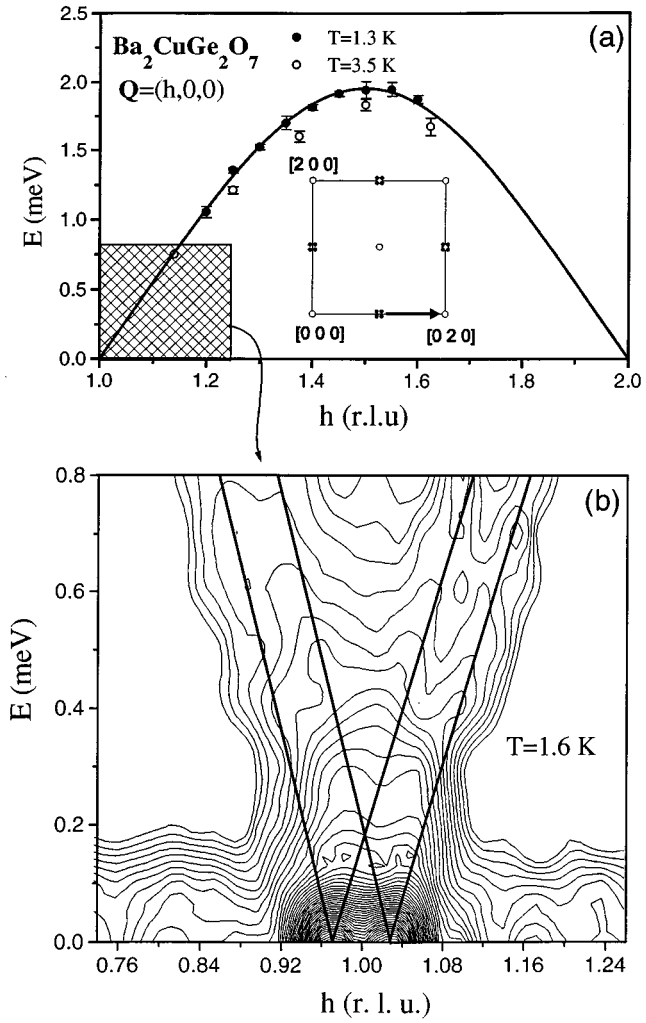

FIG. 7. (a) Spin wave dispersion relation measured in $Ba_2CuGe_2O_7$ single crystal sample along the $(h,0,0)$ direction. The data were collected using setup A at $T=1.3$ K (solid circles) and $T=3.5$ K (open circles). The solid line represents a fit to the data, as described in the text. The insert schematically shows the direction in Q space along which the dispersion was measured (open and solid circles mark the nuclear and magnetic Bragg reflections, respectively). (b) Constant-intensity contours representing the inelastic intensity I measured in constant-E scans using setup C. The contours are drawn for constant values of $\ln(I)$ in 0.2 steps.

experimental setup A, with the crystal mounted with the $(h,k,0)$ zone parallel to the scattering plane of the spectrometer. A typical constant-Q scan collected at $T=1.6$ K$<T_N$ is shown in Fig. 6(a). At this temperature the dispersion along $\mathbf{a}^*$ was found to be sinusoidal, with minima around the $(h,k,0)$ (h, k-integer) magnetic zone centers. All the experimental dispersion relations shown in this paper were obtained by fitting empirical Gaussian profile to the constant-Q inelastic data. An additional Gaussian was used in the fitting procedure to account for incoherent scattering centered at $\hbar\omega=0$. Figure 7(a) (solid circles) summarizes the results for the $(h,0,0)$ direction, $T=1.6$ K. The in-plane bandwidth is $\Delta_{\parallel}=1.95$ meV. Typical of a quasi-2D system, the higher-energy spin waves are still very well defined at $T=3.5$ K [Fig. 7(a), open symbols], i.e., above the 3D ordering temperature $T_N=3.3$ K. At this temperature the bandwidth is slightly reduced.

To measure the low-energy part of the dispersion one has to use a higher-resolution setup (paying a severe intensity penalty) to separate the spin-wave inelastic peaks from incoherent elastic scattering at $\hbar\omega=0$. These measurements were performed at $T=1.6$ K using cold neutrons in setup C. The crystal was mounted with $(h,0,l)$ wave vectors accessible for measurements. A typical constant-E scan of those utilized to measure $S(\mathbf{q},\omega)$ in the vicinity of (1,0,0) is shown in Fig. 8. A bunch of these scans collected at different energy transfer are summarized in the logarithmic intensity-contour plot in Fig. 7(b). Just discernible are the two separate spin wave branches originating from the two magnetic Bragg peaks at $(1\pm\zeta,1\pm\zeta,0)$. Note that in this geometry the magnetic Bragg peaks are out of the scattering plane. Nevertheless, the vertical Q resolution (≈ 0.05 Å^{-1} FWHM) is broad enough to capture the magnetic Bragg peaks which are seen at $\hbar\omega=0$ in Fig. 7(b).

As will be discussed below, the shape of the dispersion along $(h,0,0)$, not too close to the antiferromagnetic zone center, is only weakly affected by in-plane second-nearest neighbor (2NN) interactions. To obtain more accurate information on 2NN in-plane exchange constants some limited data were collected for the dispersion along $(h,1-h,0)$, with h around 0.5 [Fig. 9(a), open circles] using experimental setup A (crystal mounted with the $(h,k,0)$ plane horizontal).

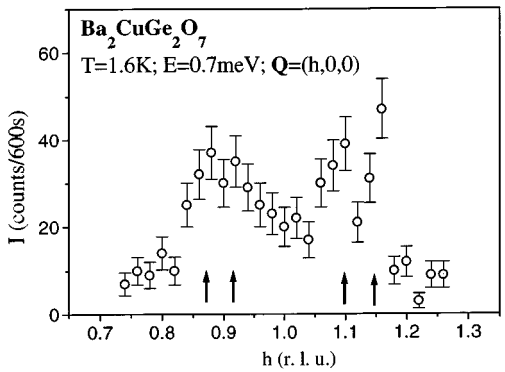

FIG. 8. Constant-E scan measured in $Ba_2CuGe_2O_7$ along $\mathbf{Q}=(h,0,0)$ at $\hbar\omega=0.7$ meV, $T=1.6$ K using setup C.

The out-of-plane dispersion (along $(1,0,l)$) was measured in constant-Q scans using setup C [typical raw data are shown in Fig. 6(b)]. The experimental dispersion relation is plotted in open symbols in Fig. 9(b).

C. Spin-wave dispersion

A look at the crystal structure of $Ba_2CuGe_2O_7$ suggests that the measured in-plane spin-wave dispersion relation should be analyzed by allowing 1NN and 2NN in-plane exchange constants J_1 and J_2.[11] For each plane the Heisenberg Hamiltonian may be written as

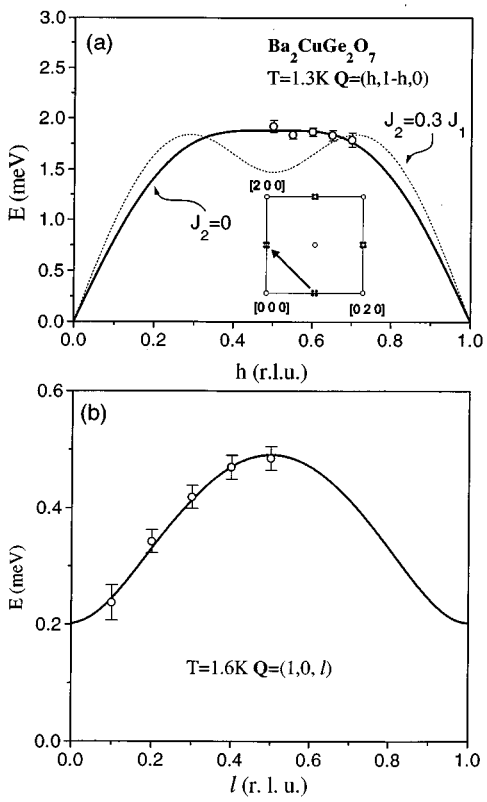

FIG. 9. Spin wave dispersion relation measured in $Ba_2CuGe_2O_7$ single crystal sample along the $(h,1-h,0)$ (a) and $(1,0,l)$ directions (b). The lines represent fits to the data described in the text.

$$\hat{H}=2J_1\sum_m\tilde{\sum_n}\,\hat{\mathbf{S}}_m\hat{\mathbf{S}}_n+J_2\sum_m\tilde{\sum_{m'}}\,\hat{\mathbf{S}}_m\hat{\mathbf{S}}_{m'}+J_2\sum_n\tilde{\sum_{n'}}\,\hat{\mathbf{S}}_n\hat{\mathbf{S}}_{n'}. \tag{2}$$

Here m and n label the spins on the two antiferromagnetic sublattices with origins at $(0,0,0)$ and $(\frac{1}{2},\frac{1}{2},0)$, respectively, and $\tilde{\Sigma}$ stands for summation over the nearest sites of appropriate sublattices. Note that in Eq. (2) every bond is counted once in the first term, twice in the second and third terms. If the incommensurability vector ζ is small, zone-boundary (short wave-length) excitations must be similar to those found in a system with a Néel ground state. For an antiferromagnet with Néel ground state linear spin-wave theory gives a rigorous expression:[12]

$$(\hbar\omega)^2=(8SJ_1)^2\left[\left(1-\frac{J_2}{J_1}\{\sin^2(\pi h)+\sin^2(\pi k)\}\right)^2-\cos^2(\pi h)\cos^2(\pi k)\right]. \tag{3}$$

A very good fit to the experimental data measured along $(h,0,0)$ is obtained assuming $J_2/J_1=0$ and $J_1=0.482(0.003)$ meV [Fig. 7(a), solid line]. We note however, that for $(h,0,0)$ magnons the shape of the dispersion curve near the zone boundary is practically independent of J_2/J_1. $(h,1-h,0)$ magnons are much more sensitive to this ratio. Fitting Eq. (3) to the experimental data collected in this direction yields $J_1=0.471(0.004)$ meV and $J_2/J_1=0.01(0.04)$. J_2 is thus too small to be a relevant parameter. The solid line in Fig. 9(a) shows the dispersion relation calculated assuming the parameters obtained from $(h,0,0)$ measurements. For comparison, a best fit with $J_2/J_1=0.3$ is shown in Fig. 9(a) in a dashed line. The in-plane spin dynamics of $Ba_2CuGe_2O_7$ not-too-close to the antiferromagnetic zone-centers is thus adequately described by *nearest-neighbor antiferromagnetic interactions alone*.

The cold-neutron inelastic data is too scarce to perform a reliable quantitative analysis and three-axis deconvolution treatment. Only a rough visual estimate [Fig. 7(b), solid lines] of the spin wave velocity $c_0\equiv d(\hbar\omega)/dh=6.0$ meV can be obtained. This is in surprisingly good agreement with the estimate that can be obtained using Eq. (3) and the refined value for J_1: $c_0=6.06$ meV. For a spiral phase we expect *two* nondegenerate spin wave branches originating from each magnetic Bragg peak.[13] One of these Goldstone modes is associated with the breaking of continuous symmetry defined by a rotation of the spin plane around the propagation vector. The other soft mode (the so-called phason) is associated with a rigid uniform rotation of the spiral *within* the spin plane. Unfortunately, the two types of magnetic excitations can not be resolved in our experiments, partly due to the overlapping signals coming from the two magnetic domains.

The transverse dispersion [along $(1,0,l)$] was analyzed using the following assumptions for the three-dimensional

spin system: Néel ground state with antiparallel in-plane nearest neighbor spins and parallel alignment of spins from adjacent planes. Using the general formula from Ref. 12, for our particular case we obtain

$$(\hbar\omega)^2=(8S)^2[J_\perp^2\sin^4(\pi l)-2J_1J_\perp\sin^2(\pi l)]+\delta_E^2. \quad (4)$$

Here $J_1=0.482$ meV and $J_\perp$ is the effective interplane ferromagnetic exchange constant ($J_\perp<0$). The gap δ_E arises from the fact that (1,0,0) is not the magnetic zone center, which is actually located at $(1\pm\zeta,1\pm\zeta,0)$:

$$\delta_E=c_0\zeta. \quad (5)$$

Using the value for c_0 obtained from measurements along $(h,0,0)$, we can estimate $\delta_E\approx 0.16$ meV. This is consistent with the value obtained by fitting the measured out-of-plane dispersion to Eq. (4) [Fig. 9(b), solid line]: $\delta_E=0.20(0.02)$ meV. The refined value for the interplane ferromagnetic exchange constant is $|J_\perp|=0.013(0.001)$ meV, roughly 37 times smaller than the in-plane exchange constant J_1.

IV. DISCUSSION

A. Powder experiments in retrospective

As mentioned in the Introduction, single crystal samples of $Ba_2CuGe_2O_7$ were initially unavailable and preliminary measurements were carried out on powders. An interpretation, totally different from the one presented in this paper, was given to the powder results.[6] For the sake of completeness we shall briefly review our powder measurements. The neutron powder diffraction profile measured using setup D at 1.4 K was at first found to be completely consistent with the crystal structure reported in Ref. 5. In particular, no magnetic Bragg reflections were found. This, we believed, spoke in favor of a nonmagnetic ground state in $Ba_2CuGe_2O_7$. Only limited inelastic powder data could be obtained. A typical constant-Q scan measured at $Q=1.0$ Å^{-1}, $T=1.4$ K using setup E is shown in Fig. 10(a). The one discernible feature of the spectrum is the broad hump seen at 1.6 meV, which at that time was interpreted as a signature of a gap in the magnetic excitation spectrum. Later, when the magnetic ordering was observed in the single-crystal sample, we have repeated the powder diffraction experiments in a limited 2θ range, greatly increasing the counting time and using experimental setup B. This enabled us to observe an extremely weak double powder peak around $Q=|a^*|$ at $T=1.5<T_N$ K [Fig. 10(b)]. Now that the spin wave dispersion was known, the inelastic peak in constant-Q powder scans was attributed to the broad plateau at $\hbar\omega\approx 1.9$ meV in the 2D dispersion manifold [Fig. 9(a)]. Powder averaging of the dynamic structure factor $S(q,\omega)$ gives rise to a peak at roughly this energy, just like a complete **Q** integration produces Van-Hove singularities. Once again the ''gap'' in the powder data illustrates how powder experiments may be misleading if the experimental resolution is a serious limiting factor (which definitely is the case for $Ba_2CuGe_2O_7$, where the spin wave bandwidth is only 2 meV).

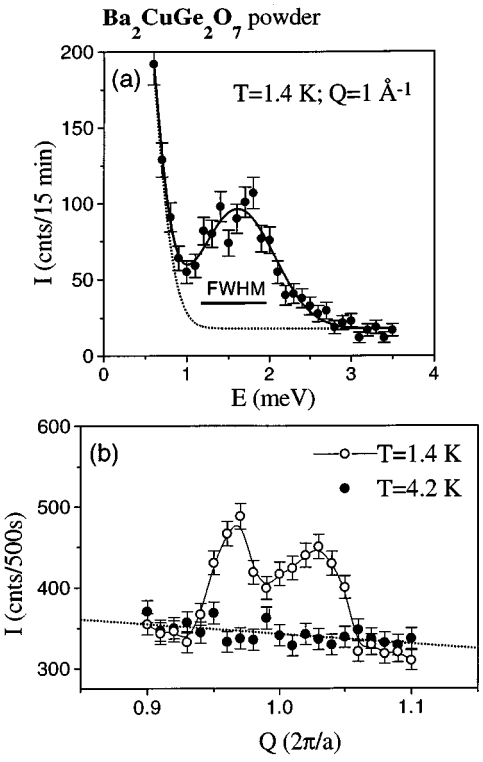

FIG. 10. (a) A typical energy scan for $Ba_2CuGe_2O_7$ powder collected at $Q=1.0$ Å^{-1}. The dashed line shows the estimated background from incoherent scattering. The solid line is a guide for the eye. (b) Elastic powder Q scans measured in a $Ba_2CuGe_2O_7$ sample at $T=4$ K (solid circles) and $T=1.4$ K (open circles). The dotted line shows the background level. The solid line is a guide for the eye.

B. Quasi-2D behavior

The measured ratio $|J_\perp|/|J_1|=1/37$ indicates that $Ba_2CuGe_2O_7$ is a ''reasonably good'' quasi-2D system. This is supported by the extremely low order-parameter critical exponent $\beta\approx 0.15$ (for a 3D Heisenberg system one expects $\beta\approx 0.35$). In a quasi-2D system 3D ordering can be viewed as secondary to the establishment of long-range order within the planes.[14] In consequence, in ''good'' quasi-2D compounds, such as K_2NiF_4,[14,15] or $Sr_2CuO_2Cl_2$,[16] 2D critical exponents are observed in a wide temperature regime even in the ordered phase. The experimental value $\beta\approx 0.15$ in $Ba_2CuGe_2O_7$ is close to $\beta=1/8$ for a 2D Ising system. It is important to note, that the critical indexes depend only on the overall symmetry of the Hamiltonian, and not on the actual magnitudes of single-ion or exchange anisotropies.[17] Therefore, the Ising-like β is not in contradiction with the Heisenberg-like magnetic susceptibility observed. Further dedicated experimental studies of the critical properties of $Ba_2CuGe_2O_7$ will undoubtedly yield interesting results.

C. Origin of the spiral phase

As shown above, the observed elastic scattering is consistent with a simple model for the spiral phase in $Ba_2CuGe_2O_7$. An early observation and theoretical study of spiral order in MnO_2 were done by Erickson[18] and Yoshimori,[19] back in 1952 and 1958, respectively. As a rule,

the primary reason for spiral ordering are competing exchange interactions. For example, spiral and helical phases in rare earths (see, for example, Refs. 20 and 21) are driven by sign-alternating, relatively long-range RKKY interactions. In a localized spin system like $Ba_2CuGe_2O_7$ or MnO_2 one can usually derive a classical spiral ground state by considering few discrete exchange coupling constants.[19]

Since in $Ba_2CuGe_2O_7$ the incommensurability vector ζ is very small, within the classical framework we can assume that the formation of the spiral *requires* that the Néel ground state is dynamically unstable. Let us consider this instability. In the most general case the classical ground state energy (per spin) is given by

$$E = S^2 \sum_{n,m,i} J(\mathbf{R}_{n,m,i}) \cos(\phi_{n,m,i}). \tag{6}$$

Here (n,m,i) is a three-dimensional index labeling the magnetic sites, where (n,m) is the in-plane index and i labels different (0,0,1) crystallographic planes $\mathbf{R}_{n,m,i}$ is the position of site (n,m,i), and $\phi_{n,m,i}$ is the angle between the (0,0,0) and (n,m,i) spins. Since the propagation vector lies in the $(h,k,0)$ plane, $\phi_{n,m,i}$ is i-independent and we can rewrite Eq. (6) as

$$E = S^2 \sum_{n,m} \widetilde{J}(\mathbf{R}_{n,m}) \cos(\phi_{n,m}), \tag{7}$$

$$\widetilde{J}(\mathbf{R}_{n,m}) \equiv \sum_i J(\mathbf{R}_{n,m,i}).$$

Note that $\widetilde{J}(\mathbf{R}_{n,m})$, the ''projected'' effective in-plane exchange constants are precisely those which determine the in-plane dispersion relation that we have measured experimentally. For the spiral phase observed in $Ba_2CuGe_2O_7$ it is trivial to rewrite Eq. (7) in terms of 1NN, 2NN, 3NN, etc., in-plane interactions $\widetilde{J}_1$, $\widetilde{J}_2$, $\widetilde{J}_3$, etc., respectively. Expanding the energy to the powers of ϕ we have

$$E \propto S^2 \phi^2 (\widetilde{J}_1 - 2\widetilde{J}_2 - 4\widetilde{J}_3 + 8\widetilde{J}_4 \cdots) + o(\phi^2). \tag{8}$$

For the Néel state to become unstable the coefficient of $(\phi)^2$ must be zero or negative. It can be seen from Eq. (8), that the larger the index k, the easier it is for k-NN interactions to destabilize the Néel phase. Our inelastic measurements near the zone boundary show that $|\widetilde{J}_2|$ and probably $|\widetilde{J}_3|$ are much weaker than $\widetilde{J}_1$. For the particular crystal geometry and in general for a localized spin system the efficacy of long-range (4NN, etc.) interactions may be expected to decrease very rapidly. Moreover, the spin wave velocity (relative to the bandwidth), should be *strongly affected* by long-range interactions, as it represents long-wavelength dynamics of the system. In $Ba_2CuGe_2O_7$ the spin-wave velocity is practically the same as the value estimated from measurements of zone-boundary magnons, for which only short-range interactions are important. These considerations suggest that long-range interactions are negligible and lead us to the conclusion that in the *classical* limit the system must have a Néel ground state, in obvious contradiction to what has been observed.

We have just shown that if $Ba_2CuGe_2O_7$ is adequately described by a Heisenberg Hamiltonian, it either has relatively strong long-range exchange interactions (in itself a remarkable phenomenon) or else the spiral phase is a manifestation of the quantum nature of the spins involved. The discovery of high-temperature superconductivity in layered cuprates and Anderson's ''resonating valence-bond'' conjecture[22] have inspired extensive theoretical studies of frustrated quantum two-dimensional Heisenberg antiferromagnets. Much attention has been given to a simple square lattice with 1NN and 2NN interactions. In the classical limit $(S \to \infty)$ a spiral phase (incidentally, exactly of the type observed in $Ba_2CuGe_2O_7$) may indeed be realized, but only for $J_2/J_1 \equiv \frac{1}{2}$.[23] For $S = 1/2$ quantum spins the spiral is stabilized in a wider range of J_2/J_1, but for $J_2/J_1 \lesssim 0.4$ it is definitely still Néel-like.[24–26] In the case of $Ba_2CuGe_2O_7$ $J_2/J_1 \ll 0.4$ and it seems unlikely that a similar mechanism could be used to explain the spiral phase involving only 1NN and 2NN in-plane interactions.

As independently suggested by Bak and Bao,[27] a very likely explanation for the origin of the spiral phase in $Ba_2CuGe_2O_7$ goes beyond the pair-spin Heisenberg exchange Hamiltonian. The situation is similar to that with MnSi:[28,29] a spiral magnetic phase with a small propagation vector is observed experimentally, but is difficult to explain in the framework of Heisenberg exchange without involving relatively strong long-range interactions. Bak and Jensen have pointed out[30] that the spiral order in MnSi and FeGe may be induced by the so-called Dzyaloshinskii-Moriya (DM) term.[31,32] The latter is of relativistic origin and is proportional to the *vector product* of interacting spins. This type of interaction introduces terms *linear* in ϕ into the classical ground state energy (8) and, no matter how weak, destabilizes the Néel phase. The DM instability is allowed by symmetry only in a noncentrosymmetric structure, which indeed is the case for $Ba_2CuGe_2O_7$ (although the arrangement of Cu^{2+} sites is centric). The rule of the thumb is that any terms allowed by symmetry must be present. Moreover, a symmetry analysis by Maslov and Bak shows that it is exactly the spiral structure observed, that is likely to be produced by DM interactions in the $Ba_2CuGe_2O_7$ structure.[27] The only unresolved question is whether Dzyaloshinskii-Moriya coupling is strong enough to induce a spiral with the observed propagation vector. The latter is plausible, since ζ is very small in $Ba_2CuGe_2O_7$.

One more remotely feasible scenario, somewhat esoteric in nature, is worth mentioning. Looking at crystal structure as depicted in Fig. 2 we see that four Cu^{2+} ions in the corners of each plaquette of the square lattice are bonded by superexchange via a Ge_2O_6 cluster symmetrically positioned in the center of the plaquette. The symmetry of this arrangement in principal allows for *four-spin exchange* terms. This type of interaction has been considered in several models of superexchange in the CuO_2 layers in high-T_C superconductors[33] and is believed to be responsible for some unusual magnetic properties of solid ^{3}He.[34] We do not know whether the four-spin term is important in $Ba_2CuGe_2O_7$, and whether it may lead to the formation of the spiral phase. However, the very structure of $Ba_2CuGe_2O_7$ suggests that four-spin effects may actually be taking place.

V. CONCLUSION

$Ba_2CuGe_2O_7$ is a very interesting quasi-2D magnetic system. It is unique in that it combines low dimensionality,

simplicity of spin arrangement, absence of an inversion center, a particular geometry of exchange pathways, and has a nontrivial incommensurate magnetic structure. Further work is bound to reveal new interesting properties of this material.

ACKNOWLEDGMENTS

We would like to thank S. Maslov, P. Bak, W. Bao, M. Hase, V. Emery, and T. Oguchi for numerous illuminating discussions. It is a pleasure to acknowledge W. Eysel for information about the crystal structure of $Ba_2CuGe_2O_7$. We also thank T. Vogt for his help with some powder diffraction experiments and H. Obara for measurements of the magnetic susceptibility below 4.2 K. This study was supported in part by NEDO (New Energy and Industrial Technology Development Organization) International Joint Research Grant and the U.S. -Japan Cooperative Program on Neutron Scattering. Work at Brookhaven National Laboratory was carried out under Contract No. DE-AC02-76CH00016, Division of Material Science, U.S. Department of Energy.

[1] M. Hase, I. Terasaki, and K. Uchinokura, Phys. Rev. Lett. **70**, 3651 (1993).
[2] M. Hase *et al.*, Phys. Rev. B **48**, 9616 (1993).
[3] Y. Sasago *et al.*, Phys. Rev. B **52**, 3533 (1995).
[4] A. Zheludev *et al.*, Phys. Rev. B **53**, 11 642 (1996).
[5] R. E. Dinnebier, Ph.D. thesis, Heidelberg University, 1993.
[6] Y. Sasago *et al.* (unpublished).
[7] J. Wang, Phys. Rev. B **44**, 2396 (1991).
[8] M. S. Makivic and H.-Q. Ding, Phys. Rev. B **43**, 3562 (1991).
[9] Y. Sasago (unpublished).
[10] P. J. Brown, in *International Tables for Crystallography*, edited by A. J. C. Wilson (Kluwer Academic Publishers, London, 1995), Vol. C, Chap. 4.4.5.
[11] The actual relevant parameters are, as defined in the discussion section, the effective 2D ''projected'' exchange constants $\widetilde{J}_1$ and $\widetilde{J}_2$ for in-plane dispersion and the 1D ''projected'' coupling constant $\widetilde{J}_\perp$ for dispersion along $(0,0,l)$.
[12] S. W. Lovesey, *Theory of Neutron Scattering From Condensed Matter* (Clarendon Press, Oxford, 1984), Vol. 2, Chap. 9.6.
[13] J. Jensen and A. R. Mackintosh, *Rare Earth Magnetism* (Clarendon Press, Oxford, 1991), Chap. 6.1.
[14] R. J. Birgeneau, H. J. Guggenheim, and G. Shirane, Phys. Rev. Lett. **22**, 720 (1969).
[15] R. J. Birgeneau, J. J. Skalyo, and G. Shirane, Phys. Rev. B **3**, 1736 (1971).
[16] M. Greven, Ph.D. thesis, Massachusetts Institute of Technology, 1995.
[17] D. Jasnow and M. Wortis, Phys. Rev. **176**, 739 (1968).
[18] R. A. Erickson, Phys. Rev. **85**, 745 (1952).
[19] A. Yoshimori, J. Phys. Soc. Jpn. **14**, 807 (1959).
[20] W. C. Koehler, J. W. Cable, M. K. Wilkinson, and E. O. Wollan, Phys. Rev. **151**, 414 (1966).
[21] W. C. Koehler *et al.*, Phys. Rev. **158**, 450 (1967).
[22] P. W. Anderson, Science **235**, 1196 (1987).
[23] P. Chandra and B. Doucot, Phys. Rev. B **38**, 9335 (1988).
[24] J. H. Xu and C. S. Ting, Phys. Rev. B **42**, 6861 (1990).
[25] E. Dagotto and A. Moreo, Phys. Rev. Lett. **63**, 2148 (1989).
[26] E. Dagotto and A. Moreo, Phys. Rev. B **39**, 4744 (1989).
[27] P. Bak and W. Bao (private communication).
[28] Y. Ishikawa, K. Tajima, D. Bloch, and M. Roth, Solid State Commun. **19**, 525 (1976).
[29] G. Shirane *et al.*, Phys. Rev. B **28**, 6251 (1983).
[30] P. Bak and M. H. Jensen, J. Phys. C **13**, L881 (1980).
[31] I. E. Dzyaloshinskii, JETP **46**, 1420 (1964).
[32] T. Moriya, Phys. Rev. **120**, 91 (1960).
[33] M. Roger and J. M. Delrieu, Phys. Rev. B **39**, 2299 (1989).
[34] J. M. Delrieu, J. Low. Temp. Phys. **40**, 71 (1980).